

Copyright 2001, Society of Photo-Optical Instrumentation Engineers

This material was presented at SPIE's Lithography for Semiconductor Manufacturing II conference as paper 4404-33 and is made available as an electronic reprint with permission of SPIE. One print or electronic copy may be made for personal use only. Systematic or multiple reproduction, distribution to multiple locations via electronic or other means, duplication of any material in this paper for a fee or for commercial purposes, or modification of the content of the paper are prohibited.

Optical proximity strategies for desensitizing lens aberrations

John S. Petersen

ABSTRACT

The use of image process integration to minimize the effect of lens aberrations on the microlithographic imaging process is briefly surveyed. Examples show how field of curvature, focus and spherical aberrations can be minimized by using off-axis illumination and scattering bar OPC. Sub-resolution assist features redistribute the energy within the pitches' diffraction pattern, reducing the weighted average aberration. A demonstration of the use of scattering bars to balance the magnitude of aberrated diffraction orders to correct focus shifts of isolated to semi-isolated features is provided. This example shows the impact of symmetric aberrations on 100 nm images produced using off-axis 248 nm illumination, 0.7 numerical aperture and chromeless phase-shift mask for pitches of 260 nm, 300 nm, 350 nm, 400 nm, 500 nm, 600 nm, 1200 nm and 10000 nm.

Keywords: image process integration, phase-shift mask, microlithography, optical lithography, resolution enhancement technique, RET, PSM, off-axis illumination, OAI, scattering bars, sub-resolution assist features, optical proximity correction, OPC, 100 nm lithography

1. INTRODUCTION

The use of resolution enhancement techniques has made it necessary to understand the effect of aberrations for advanced imaging to be achieved. Previous work discusses how illuminator shape and mask type/design affect aberrations, and how they use the lens and pupil when paired with Köhler illumination.^{1 2 3 4} This provides a brief survey of effective techniques and considers how to desensitize an integrated imaging process to aberrations in the projection system.

Simply put, beams of a diffraction pattern projected through a perfect lens create a very precise image where the diffraction orders interfere at the image plane. When there are aberrations in the lens, the beams converge but never quite form a precise point (Figure 1). Instead, they are slightly blurred into what is sometimes called "circle confusion." Even for a corrected lens, what we call "best focus" is actually the area of least confusion for all aberrations. Generally speaking, there are three families of aberrations: monochromatic, chromatic, and defocus. Within monochromatic aberrations there are spherical, coma, astigmatism, field of curvature, and distortion.^{5 6} We will concentrate on spherical, field of curvature, and defocus aberrations.

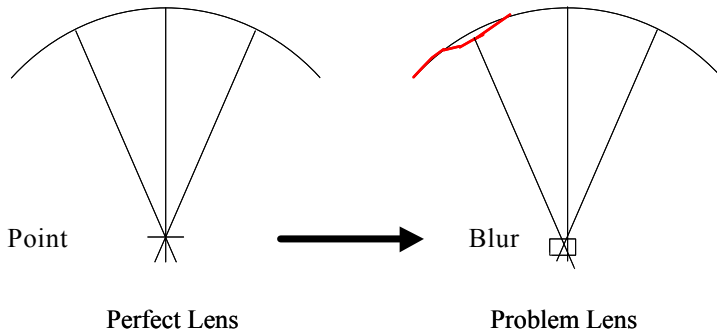


Figure 1: Perfect lens and aberrated lens

Aberrations are problematic because they reduce the working resolution of the imaging system. In a 1989 paper, I showed the process windows for four different feature sizes of k_1 : 0.771, 0.690, 0.661 and 0.592.⁴ These showed good process window symmetry (meaning that when out of focus the CD contours behave in similar fashion) for the larger 0.771 k_1 feature, but with each correspondingly smaller k_1 , asymmetry about the center of focus became more prominent. An interesting aspect of these data was that the features shown actually consisted of two different pitches imaged at two different NAs on the same exposure tool. So, for each respective pitch, there was a different sampling of the diffraction pattern through the same aberrated lens (Figure 2). It would seem, then, that the loss of symmetry in the process window is due to an across-source unbalancing of the aberrations within the system. This phenomenon has been described by Smith³ and Proglor⁵ and, with respect to these data, may be one significant reason why tool manufacturers specified 0.8 k_1 lenses for so many years.

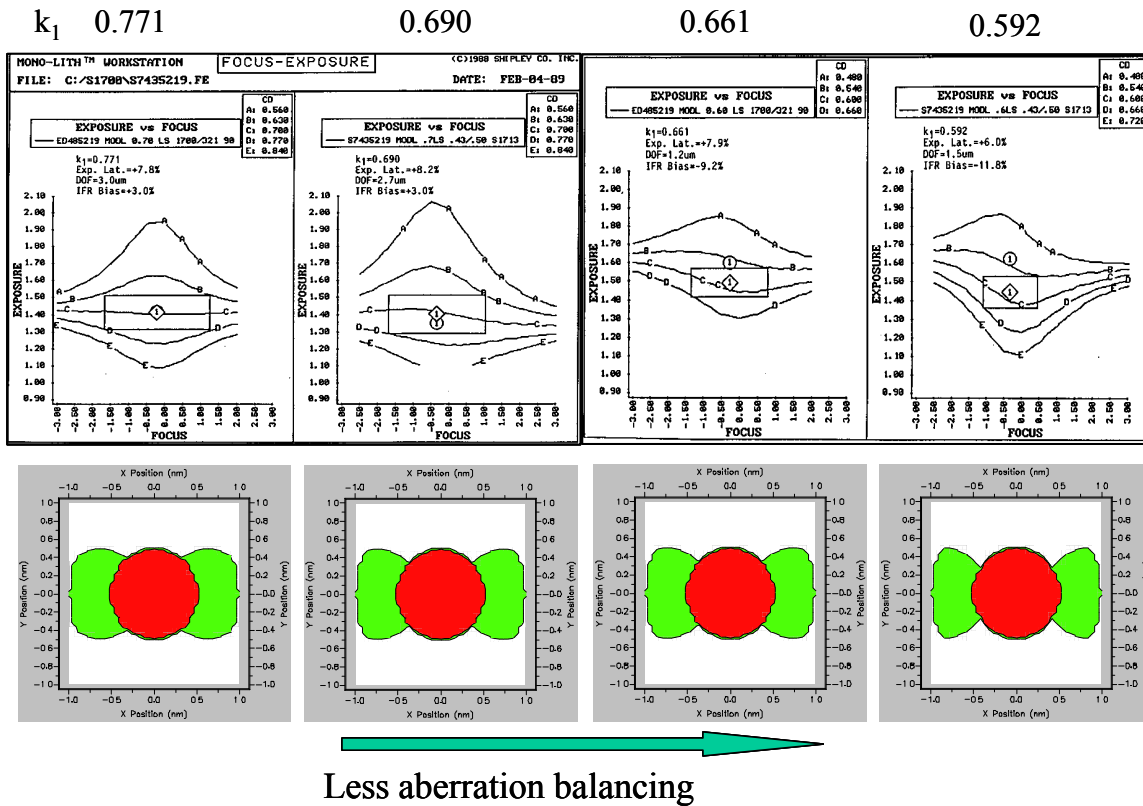


Figure 2: Process window loss with aberrations⁴

Reducing the effects of aberrations is key to improving the working resolution of an imaging system—as important as using phase-shift masks, off-axis illumination, or the other resolution enhancement techniques. It has been discussed that for a certain set of exposure tools, the full field working resolution is as much as 20 percent poorer than could be achieved for any single point in the field. Further, reducing the effect of aberrations by 11 to 12 percent could gain nearly 13 percent in working full field resolution.⁶

To limit aberrations, we must use the concept of Image Process Integration (IPI) to form an integrated imaging system that will allow us to attain full field resolution of the smallest possible features using our current optical printers. IPI seeks to find a synergistic optimum between the exposure tool, layout/design, mask, resist, and wafer. In this paper we will examine the methods and tools needed to use IPI to attack aberrations. We will consider what can be done with illumination, scattering bars and phase-shift masks. Finally, we will estimate aberrations using lithographic response of center and depth of focus for different pitches of 100 nm lines, and then simulate mask modifications to improve performance across multiple pitches.

2. SURVEY OF SUCCESSFUL TECHNIQUES

A key component for improving the working resolution of an imaging system is to move from a three-beam imaging process to a two-beam imaging process (Figure 3).^{7,8} The reason is that a three-beam imaging system provides only a very narrow range in which the zero and first diffraction orders remain in phase, limiting depth of focus. This limitation is overcome using the two beam imaging system—as long as there is temporal and spatial coherence the diffraction patterns are in phase and will interfere properly. Two-beam imaging systems are formed either by using strong phase shifters or by using three-beam imaging systems with an off-axis illumination source. When using a dual-exposure technique with alternating phase shift masks (strong shifters), layout constraints restrict the number of devices that fit in a given area⁹. Consequently, we will limit our discussion to off-axis illumination solutions with weak phase shift masks.

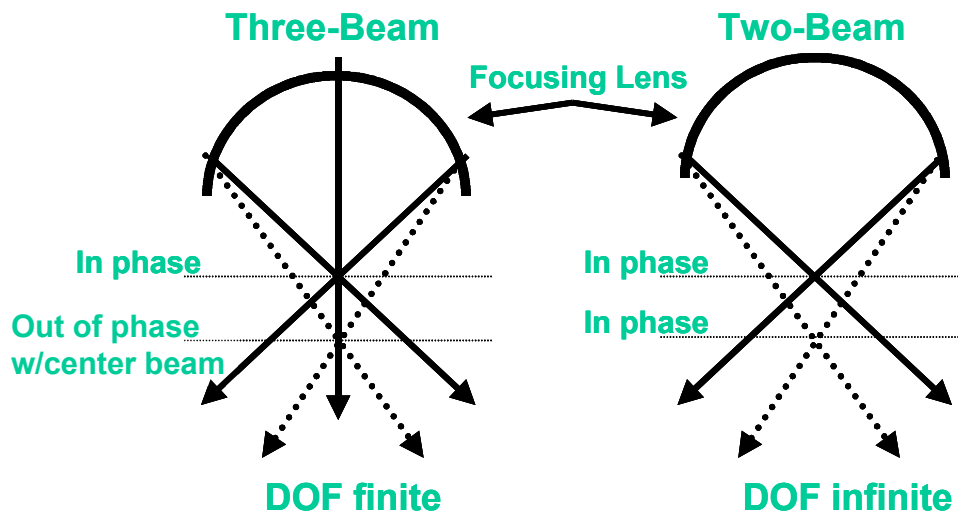


Figure 3: Two- and three-beam imaging

One of the first ways to minimize the impact of lens aberrations is to use off-axis illumination to improve the overall process window. There are two types of off-axis illumination: strong and weak. Strong illuminators have no intensity between the poles. Weak illuminators have a non-zero intensity between the poles. Figure 4 maps depth of focus for quarter micron contact holes imaged with conventional illumination (sigma: 0.74, numerical aperture: 0.53, resist: Shipley UVIIHS, dose: 15.5mJ). The rows represent the focus setting and the columns represent the reticle field position shown in Figure 5. They are oriented so that field curvature, if any, is displayed.

Cells with shaded backgrounds represent measurements that are within the +/- 10 percent critical dimensions back. The conventional illumination provides no common depth of focus across the 22 mm field and only 0.1µm for the 15 mm diameter. These results are largely due to a field of curvature aberration in the lens.

focus/zone	BL	TL	BLZ	TLZ	BLM	TLM	Axis	BRM	TRM	BRZ	TRZ	BR	TR
-0.85													
-0.8													
-0.75													
-0.7													
-0.65													
-0.6													
-0.55													
-0.5													
-0.45													
-0.4													
-0.35													
-0.3													
-0.25					0.217	0.193	0.195						
-0.2			0.189	0.187	0.226	0.222	0.226		0.209				
-0.15	0.188	0.206	0.209	0.214	0.242	0.245	0.242		0.236				
-0.1	0.206	0.225	0.221	0.231	0.253	0.253	0.256	0.211	0.245		0.201		
-0.05	0.222	0.228	0.234	0.242	0.262	0.257	0.258	0.232	0.256		0.235		0.195
0	0.236	0.21	0.245	0.226	0.254	0.237	0.263	0.253	0.252	0.197	0.254		0.237
0.05	0.231		0.241	0.206	0.229	0.229	0.249	0.256	0.247	0.234	0.267	0.191	0.239
0.1	0.221		0.237		0.216	0.205	0.237	0.258	0.239	0.252	0.253	0.222	0.253
0.15	0.194		0.218				0.222	0.247	0.229	0.258	0.242	0.234	0.247
0.2			0.193					0.233	0.205	0.251	0.222	0.247	0.231
0.25								0.221		0.232		0.214	0.216
0.3										0.219		0.185	
0.35													
0.4													
0.45													

Field of Curvature

Figure 4: Conventional illumination 250 nm contact holes depth of focus

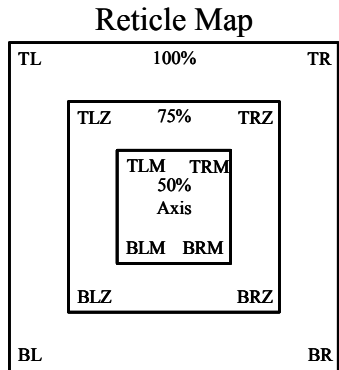


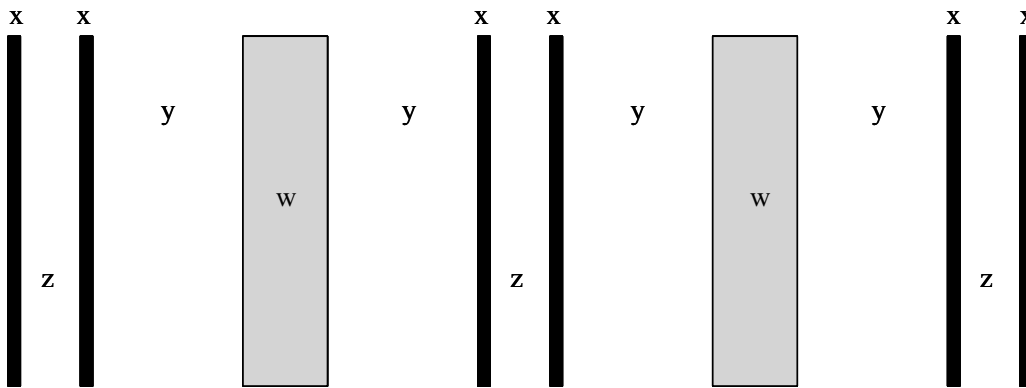
Figure 5: Reticle map

Using the same lens with off-axis, quadrupole illumination (center sigma: 0.59, radial sigma: 0.15, dose: 19mJ) the process window within each field point greatly increases, yielding 0.55µm depth of focus at 22 mm field, 0.7µm depth of focus at the 17.5 mm field, and 0.9µm depth of focus at the 15 mm field (Figure 6). Thus by changing illumination we gained depth of focus without changing the curvature of the lens.²

focus/zone	BL	TL	BLZ	TLZ	BLM	TLM	Axis	BRM	TRM	BRZ	TRZ	BR	TR
-0.85											0.221		
-0.8											0.235		
-0.75		0.197	0.213								0.238		
-0.7		0.225	0.226	0.222							0.241		
-0.65		0.229		0.229	0.213		0.245				0.249		
-0.6		0.239		0.243	0.229	0.214	0.249	0.199	0.201	0.201	0.252		
-0.55				0.248	0.238	0.231	0.251	0.229	0.227	0.221	0.251		
-0.5	0.198			0.258	0.239	0.246	0.259	0.236	0.248	0.237	0.255	0.228	
-0.45	0.215			0.256	0.252	0.253	0.263	0.246	0.255	0.249	0.259	0.249	
-0.4	0.227			0.262	0.251		0.264	0.252	0.258	0.252	0.261	0.253	0.244
-0.35	0.236			0.265	0.257		0.259		0.256	0.254	0.263	0.259	0.247
-0.3	0.242			0.266			0.262		0.253	0.256	0.262	0.265	0.243
-0.25	0.246	0.255		0.268			0.266		0.262	0.254	0.265	0.266	0.252
-0.2		0.251	0.262	0.269			0.268		0.264	0.251	0.267	0.259	0.254
-0.15		0.252	0.256	0.264			0.273		0.265	0.252	0.266	0.263	0.259
-0.1		0.248	0.258	0.255			0.271		0.266	0.246	0.268	0.259	0.262
-0.05			0.251	0.257		0.266	0.268		0.267	0.249	0.265	0.262	
0	0.248		0.246	0.261	0.267	0.26	0.267	0.264	0.264	0.248	0.263	0.252	0.261
0.05	0.242		0.248	0.256	0.262	0.261	0.263	0.261	0.264	0.243	0.261	0.248	0.256
0.1	0.241		0.238	0.249	0.257		0.256	0.259	0.259	0.234	0.255	0.247	0.254
0.15	0.237		0.234	0.255			0.258	0.252	0.261	0.23	0.249	0.254	0.255
0.2	0.226	0.214	0.225	0.239			0.256		0.254	0.225	0.246	0.239	0.248
0.25	0.214	0.191	0.211	0.231			0.251		0.252	0.214	0.239	0.243	0.236
0.3	0.195			0.214			0.249	0.249	0.247	0.196	0.236	0.228	0.209
0.35					0.251		0.245	0.242	0.245		0.227		
0.4					0.231	0.235	0.232	0.223	0.229		0.221		
0.45					0.211	0.221	0.216	0.205	0.212		0.214		

Figure 6: Quadrupole illuminator, 250 nm contact holes depth of focus

Scattering bars (also called “sub-resolution assist features”) are illustrated in Figure 7. The OPC technique consists of placing sub-resolution features on each side of a wider primary feature. If the primary feature is isolated, multiple scattering bars can be used.¹⁰



$$w=160\text{nm}; x=60\text{nm}; y=300\text{nm}; z=80\text{nm}$$

Figure 7: Scattering bars

Without redoing the mathematics, scattering bars basically push the energy from the center of the lens to the outer edge of the lens, forcing a discrete isolated pattern to behave as a dense line pattern (Figure 8).¹¹ Note the loss of amplitude at the center of the lens and the larger amplitude of the second order for the smaller pitch. Figure 9 (modified from Figure 12) compares the process window for a conventional illumination scheme with no scattering bars with annular illumination using scattering bars. Note that the conventional illumination has an asymmetric process window, whereas the annular illumination with scattering bars has a process window with greater symmetry and a larger common corridor. These results are consistent with others’ results.^{12 13 14}

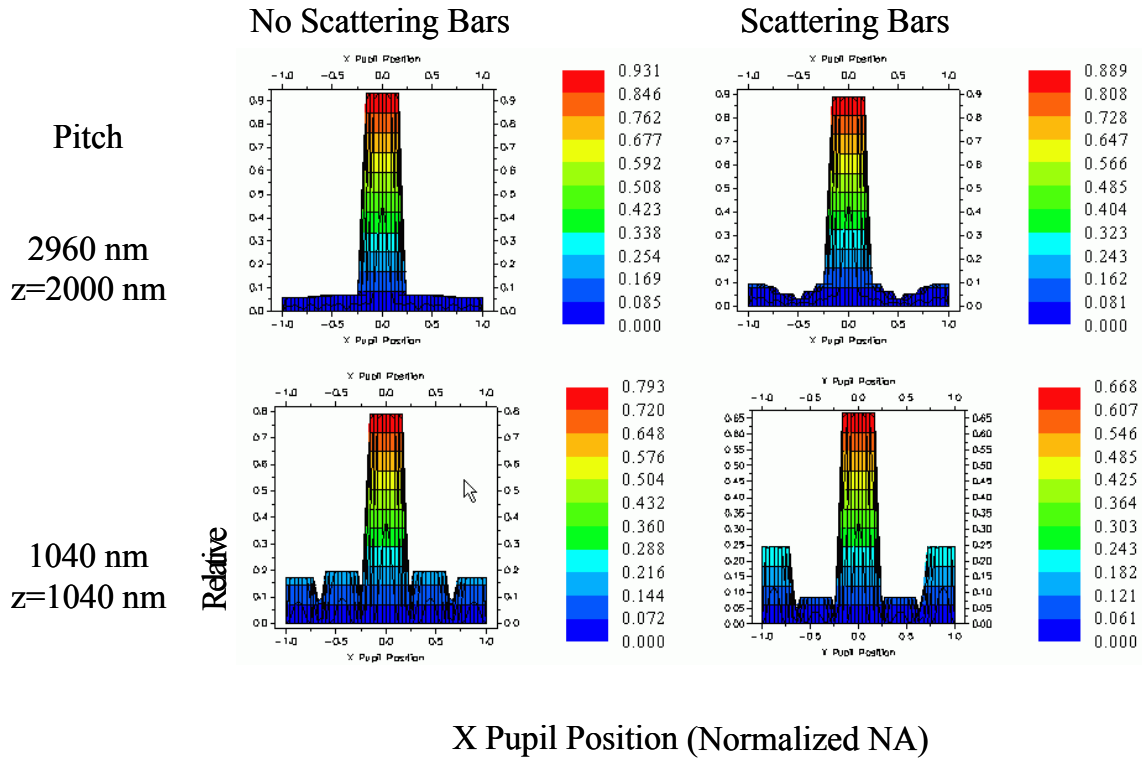


Figure 8: Electric field amplitude for isolated features with and without scattering bars

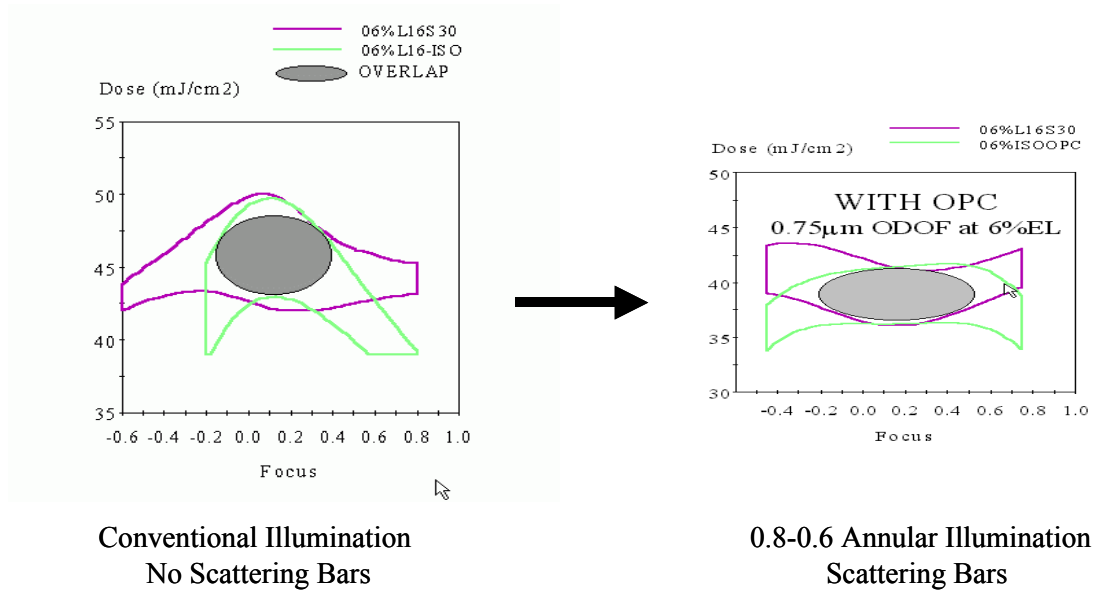


Figure 9: 160 nm lines imaged using 0.6 NA with conventional illumination (without scattering bars) and 0.8-0.6 annular illumination (with scattering bars)¹¹

Use of a weak illuminator can improve the common process corridor for different pitches. Figure 10, courtesy of J. Fung Chen et.al.⁹, shows the linewidth with changes in focus for a 420 nm pitch structure and a 720 nm pitch structure with and without scattering bars.

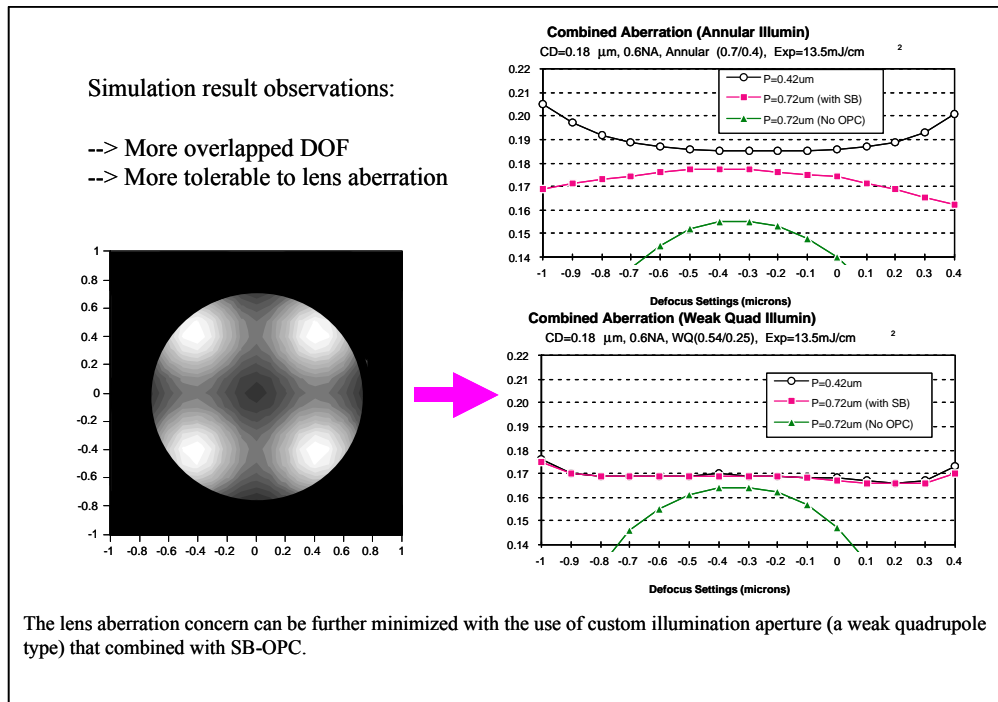


Figure 10: Common corridor for multiple pitches using scattering bars⁹

With annular illumination, the 420 nm pitch and the 720 nm pitch with scattering bars have nearly the same process region, but the isolated feature without scattering bars does not. The process can be improved further using a weak quadrupole illuminator, which brings the dense and isolated features closer together such that the dense feature and the isolated feature with scattering bars share the same process region.

As demonstrated above, scattering bars can substantially improve performance. However, other techniques also can help desensitize aberrations. Ma showed that chrome frames could be used to desensitize aberrations when imaging contact holes with phase shift masks.¹⁵ Socha et.al. used simulation to show that alternating phase shift masks and high transmission phase shift masks can also limit aberrations.¹⁶

Phase shift masks using scattering bars combined with off-axis illumination is known to be effective in improving the common process window between dense and isolated features.¹¹ Because they improve multiple pitch focus-exposure performance, scattering bars also improve performance with respect to aberrations.⁹ Improving the process window size is not only way scattering bars help limit the effect of aberrations, though, as we will demonstrate.

As an example, we analyzed a hypothetical set of diffraction patterns for 100 nm line and space features. The results were generated using full vector (unpolarized) PROLITH models set for a high contrast ($n=34$) resist and diffusion length of 30 nm, the Zernikes chosen were -0.07 waves of Z9. The hypothetical tool is a 0.7 NA, 248 nm with QUASAR illuminator with inner sigma of 0.55, outer sigma of 0.85 and 30° side boundaries. The

simulated mask was a chromeless phase-shift with biasing and π -shifted sub-resolution assist features and the 100 nm line pitches simulated were 260 nm, 300 nm, 350 nm, 400 nm, 500 nm, 600 nm, 1200 nm and 10000 nm.

Figure 11 shows diffraction patterns for 100 nm lines for 300 nm, 350 nm, 500 nm, and 600 nm pitches. Of these pitches, the 350 nm shows the best symmetry of interfering beams around the optical axis, since it has the best overlay of the zero and opposing pole's first order. This pitch samples the fewest aberrations, and, in a thin resist, the center of focus will be near that of the aberrations it samples. In the other pitches, the zero and higher orders are spread over more of the lens, so all the coherently linked points will sample a wider range of aberrations, causing the center of focus to shift from pitch to pitch. Corresponding amplitudes are shown in Table 1; as expected the 600 nm pitch with scattering bars has the lowest first order magnitude.

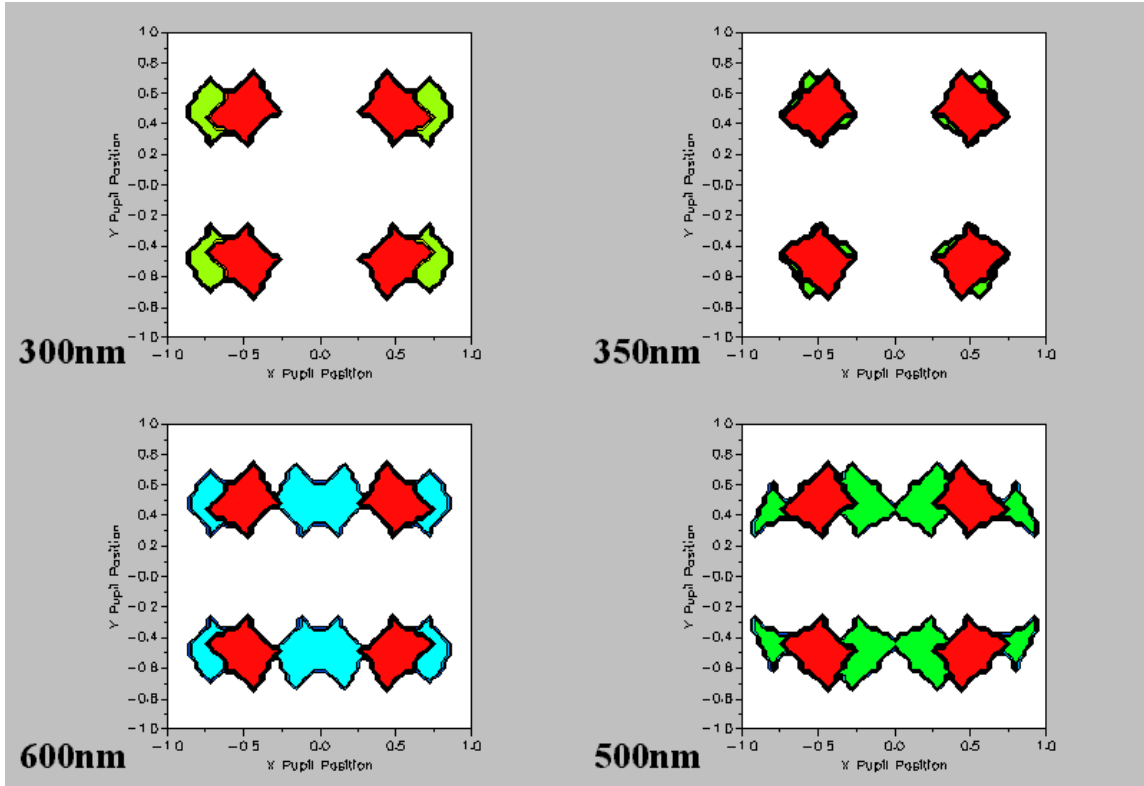


Figure 11: Diffraction pattern of 100 nm lines

Pitch (nm)	OPC	Electric Field Magnitude		
		Zero Order	First Order	Second Order
300	Bias	0.505	0.374	
350	Bias	0.657	0.327	
500	Bias	0.680	0.307	0.269
600	π -Scatter Bar/Bias	0.702	0.119	0.274

Table 1: Electric field magnitude of diffraction orders falling within the lens

Of particular interest are the 300 nm and the 600 nm pitches. The 300 nm pitch's first and 600 nm pitch's second orders sample the same parts of the lens, but, as Figure 14 will show, they have different centers of focus. It is probable that the 600 nm pitch's first order is counterbalancing the effect of its second order, thus providing a shift to the positive center and yielding a center of focus near $0\mu\text{m}$. If so, then using scattering bars on the 500 nm pitch to increase the effect of its second order may pull its center of focus back to zero from $-0.12\mu\text{m}$.

Figure 12 shows the 350 nm pitch and the 500 nm pitch diffraction patterns superimposed upon the -0.07 waves of Z9. As discussed, the 350 nm pitch diffraction pattern uniformly samples the aberration, reducing the spherical effect and making the center of focus equal to $0\mu\text{m}$. However for the 500 nm pitch, in which energy is balanced among the higher diffraction orders, a larger range of the aberration is sampled, resulting a shift in center of focus⁵, as shown in Figure 14.

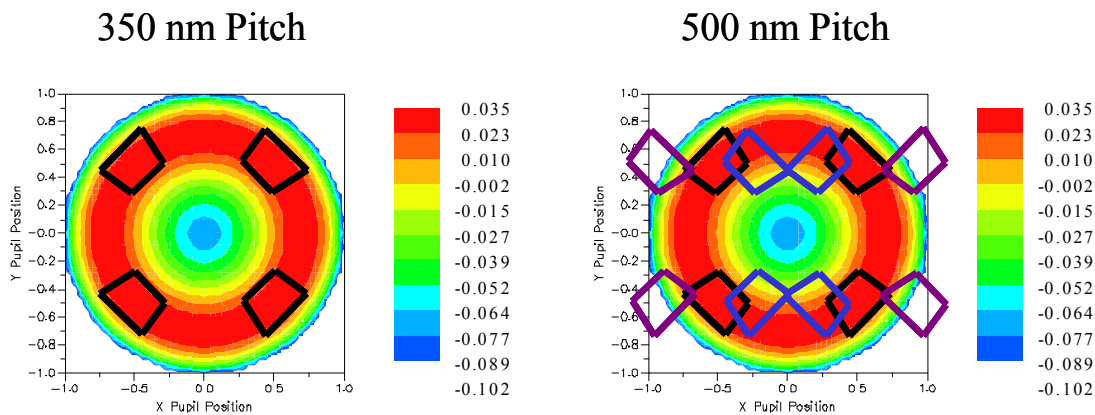


Figure 12: 350 nm and 500 nm diffraction patterns superimposed on -0.07 waves of Z9

Figure 13 shows the diffraction pattern for the 500 nm pitch with and without scattering bars. Adding the π -shifted scattering bars reduced the amplitude of the electric field from 0.680 to 0.547 for the zero order, and from 0.307 to 0.182 for the first order, but increased the amplitude for the second order from 0.269 to 0.370. Our simulation suggests that adding the appropriate assist features brings the center of focus close to $0\mu\text{m}$, improving the focus across pitch common corridor.

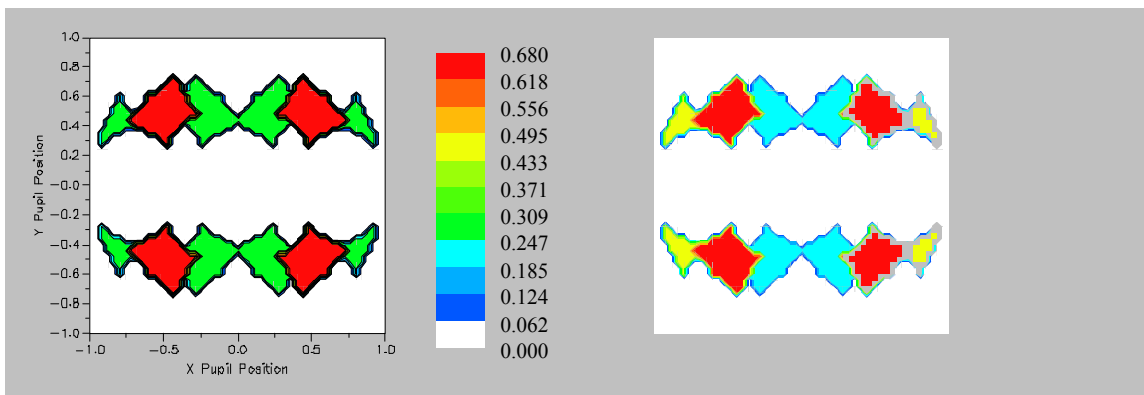


Figure 13: 500 nm pitch diffraction patterns without and with scattering bars

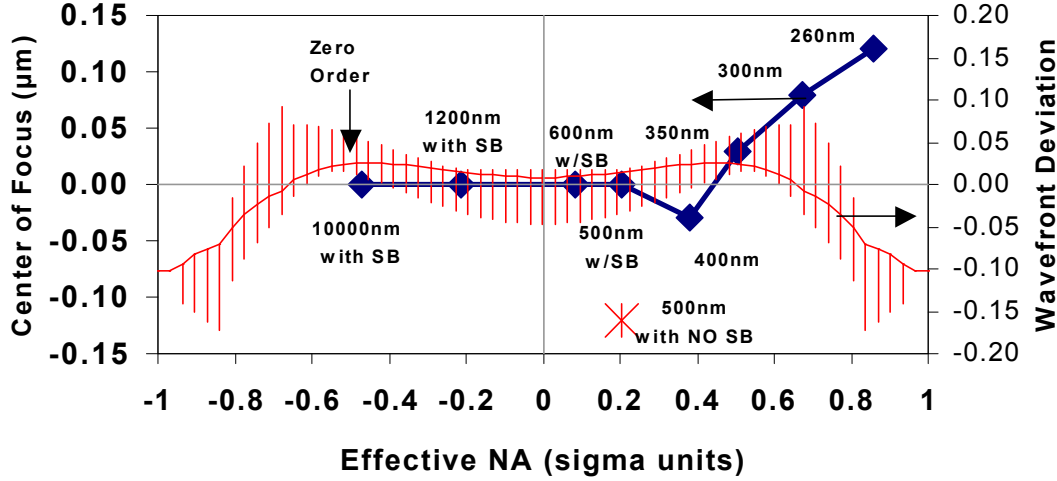


Figure 14: Simulated center of focus (left vertical axis) for different pitches and wavefront (right vertical axis) deviation plotted versus the effective NA. The vertical bars represent the range of aberration above and below the average.

The center of focus for each pitch versus effective numerical aperture is shown in Figure 14; also shown is a plot of -0.07 waves of phase error. The effective NA is used because it shows in the frequency domain where the center of the zero and first order energy samples the lens.

The center of focus in Figure 14 changes across pitch because of aberrations sampled by the interfering beams as they pass through the lens.^{3 5} This figure shows the simulated center of focus (left vertical axis) for different pitches (as labeled) and wavefront deviation (right vertical axis) plotted versus the effective NA. The vertical bars represent the range of aberration above and below the average. The diamonds in the figure correspond to the coordinate pair (Effective NA, Center of Focus) where $\text{Effective NA} = \lambda / (\text{Pitch} \cdot \text{NA}) - \sigma_{\text{QUASAR}}$

and where the center of the first order samples the lens at a constant σ_{y_QUASAR} for any σ_x .

The effect of aberrations on center of focus will be the wavefront deviation between zero order at

$\sigma_x = \sigma_y = \sqrt{\sigma_{\text{center}}^2} / 2 \cong 0.5$ and the effective NA of the first order. For higher orders, it is useful to observe that the 1200 nm pitch has the same effective NA as the 600 nm's first order, and its third order matches the first order of the 300 nm pitch. Similarly, the 600 nm's second order matches the effective NA of the 300 nm pitch's first order. Each order relative to its aberration and magnitude will affect center of focus. In this figure the 300 nm and 260 nm pitches have the largest difference in aberrations in the first order, and thus the largest shift in center of focus. The 400 nm pitch has the largest deviation with the second order, followed by the 500 nm pitch; in comparison with the 500 nm pitch, the 400 nm pitch feature has little of the second order in the lens to affect center of focus. Consequently, the aberrated second order diffraction pattern will have a lesser effect on the center of focus for the 400 nm pitch feature than for the 500 nm.

The 500 nm pitch feature without scattering bars has a negative center of focus, having followed a downward trend that spans across the 260, 300, 350, and 400 nm pitch features. From observing the 260 nm pitch, we know that the aberration sampled by its first order yields a highly positive center of focus. For the 500 nm pitch, a very similar aberration is sampled by the second order, but in only a small amount. If we can increase the amount of second order energy affected by the positive-yielding aberration, the center of focus for the 500 nm should move closer to zero. To do this, we add scattering bars.

Adding scattering bars can reduce the weighted average aberration. The question then becomes, what happens if another lens with different aberrations were used? Would the enhanced mask design still provide the desired across-pitch performance? To answer this question, we simulated the center of focus at three levels of aberration (0.00, -0.007, -0.07 waves) for Z7 (coma) and Z9 (spherical). This was not a full-factorial analysis because of the order of magnitude used—instead we examined each aberration separately and paired with its equivalent magnitude. The results (Table 2) showed that the corrected mask worked for both Z7 and Z9, because although the -0.070 wave aberration was not corrected for the smaller pitches, the larger pitches retained a center of focus close to zero. In other words, rebalancing the diffraction pattern using scattering bars did not negatively impact the common corridor for any of the aberrations examined. Table 2 also shows that with respect to the center of focus, the 500 nm pitch definitely needs the π -scattering bars, and, as expected from Figure 14, the 600 nm pitch needs them to a lesser degree.

Z7	Z9	Pitch (nm)			
		260	300	500	600
0.000	0.000	0.00	0.00	0.00	0.00
-0.007	0.000	0.00	0.00	0.00	0.00
-0.070	0.000	0.00	0.00	0.00	0.00
-0.007	-0.007	0.00	0.00	0.00	0.00
-0.070	-0.070	+0.11	+0.08	+0.01	+0.01
0.000	-0.070	+0.12	+0.08	0.00	+0.01
0.000	-0.007	0.00	0.00	0.00	0.00
0.000	-0.070	X	X	-0.10 (no SB)	-0.04 (no SB)

Table 2: Center of focus for four different pitches and different levels of Z7 and Z9. The last row shows the 500 and 600 nm pitch with bias but no δ -scattering bars. Simulated with PROLITH 3D v. 7.0, imaging model: unpolarized vector, speed factor: 4, LPM: diffusion length: 30 nm, contrast: 34.

4. CONCLUSION

While resolution enhancement techniques can greatly improve imaging, it is important to get the most out of the lens by minimizing the effects of aberrations. This can be done through proper design of both the illuminator and the mask. In this paper we showed how using off-axis illumination can improve performance both by increasing the size of process window and by changing how symmetrical lens aberrations are sampled. It was also shown for sub 100 nm features how to further desensitize imaging to lens aberrations by manipulating the magnitude of the diffraction orders by using phase shift masks and scattering bars.

5. ACKNOWLEDGEMENTS

I would like to thank Fung Chen of ASML MaskTools and Robert Socha of ASML for many excellent discussions concerning aberrations, scattering bars and microlithography. Further, I would like to thank FINLE Technologies' for the use of PROLITH. I would also like to thank Carita Simons of PAL for her edits and technical writing of this paper.

REFERENCES

-
- ¹ B.W. Smith, "Variations to the influence of lens aberration invoked with PSM and OAI" SPIE Vol. 3679, pp.330-346, 1999.
- ² B.W. Smith and J.S. Petersen, "Influences of OAI on optical lens aberration," J.Vac.Sci. Technol. B 16(6) p. 3405, 1998.
- ³ B.W. Smith and Ralph Schlieff, "Understanding lens aberration and influences to lithographic imaging", SPIE Vol. 4000, pp. 294-306, 2000.
- ⁴ J. S. Petersen, "Experimental determination of the optical lithographic requirements for sub-micron projection printing" SPIE Vol. 1088, p. 540-567, 1989
- ⁵ Christopher Progler and Donald Wheeler, "Optical lens specifications from the user's perspective", SPIE Vol. 3334, pp.256-268, 1998.
- ⁶ John S.Petersen, Martin McCallum, Nishrin Kachwala, Robert J Socha, Jang Fung Chen, Tom L Laidig, Bruce W Smith, Ronald L Gordon, Chris A Mack, "Assessment of a hypothetical roadmap that extends optical lithography through the 70-nm technology node", SPIE Vol. 3546, pp. 288-303, 1998.
- ⁷ C.A. Mack, KTI Microlithography Seminar Interface '89, pp.209-215, 1989.
- ⁸ D.L. Fehrs, H.B. Lovering, R.T. Scruton, KTI Microlithography Seminar Interface '89, pp. 217-230, 1989.
- ⁹ J. Fung Chen, T. Laidig, K. E. Wampler, R. Caldwell, K. H. Nakagawa, A. Liebchen, "A Practical Technology Path to Sub-0.10 Micron Process Generations Via Enhanced Optical Lithography", *1999 Semiconductor Technology T-CAD Workshop and Exhibition* Vol. 3, Hsin-Chu, Taiwan, section 8, paper 2 (1999).
- ¹⁰ J. Petersen, "Analytical Description of Anti-Scattering and Scattering Bar Assist Features", SPIE Vol. 4000, pp. 77-89, 2000 and references therein.
- ¹¹ Nishrin Kachwala, John S. Petersen, J. Fung Chen, Mike Canjemi, Martin McCallum, "Imaging contrast improvement for 160-nm line features using subresolution assist features with binary, six percent ternary attenuated phase-shift mask with process-tuned resist" SPIE Vol. 3679, pp. 55-69, 1999.
- ¹² Kent H. Nakagawa, Uwe Hollerbach, J. Fung Chen, "The Effects of Off-Axis Illumination and Scattering-Bar Optical Proximity Correction on the Impact of Lens Aberration on 130nm Poly Gate Mask—A Simulation Study", SPIE Vol. 4800, pp. 1070-1078, 2000.
- ¹³ Manhyooung Ryoo, Dongseok Nam, Hanku Cho, Jootae Moon, Sangin Lee, "Pattern Asymmetry Correction Using Assist Patterns", SPIE Vol. 4000, pp. 307-314, 2000.
- ¹⁴ Scott M. Mansfield, Lars W. Liebmann, Antoinette F. Molless, Alfred K. Wong, "Lithographic Comparison of Assist Feature Design Strategies", SPIE Vol. 4000, pp. 63-76, 2000.
- ¹⁵ Z. Mark Ma, Andrew Andersson, "Preventing sidelobe printing in applying attenuated phase-shift reticles", SPIE Vol. 3334, pp. 543-552, 1998.
- ¹⁶ Robert J. Socha, Will E. Conley, Xuelong Shi, Mircea V. Dusa, John S Petersen, Jang Fung Chen, Kurt E. Wampler, Tom L Laidig, Roger F. Caldwell, "Resolution enhancement with high-transmission attenuating phase-shift masks", SPIE Vol. 3748, pp. 290-314, 1999.